Journal of Geophysical Research: Space Physics

RESEARCH ARTICLE
10.1029/2018JA026074

Special Section:
Particle Dynamics in the Earth's Radiation Belts

Key Points:
- The initial enhancements of ~30-keV to 2-MeV electrons are always located outside of the innermost plasmapause locations
- The initial enhancement of >800-keV electrons always occurs at ~1.5 R_E away from the 12-hr innermost plasmapause locations
- A drastic difference of the energy spectrum evolution between inside and outside of the plasmasphere is observed during storm periods

Supporting Information:
- Supporting Information S1

Correspondence to:
L. Y. Khoo,
leng.khoo@lasp.colorado.edu

Citation:
Khoo, L. Y., Li, X., Zhao, H., Sarris, T. E., Xiang, Z., Zhang, K., et al. (2018). On the initial enhancement of energetic electrons and the innermost plasmapause locations: Coronal mass ejection-driven storm periods. *Journal of Geophysical Research: Space Physics*, *123*. https://doi.org/10.1029/2018JA026074

Received 10 SEP 2018
Accepted 23 OCT 2018
Accepted article online 26 OCT 2018

©2018. American Geophysical Union. All Rights Reserved.

On the Initial Enhancement of Energetic Electrons and the Innermost Plasmapause Locations: Coronal Mass Ejection-Driven Storm Periods

Leng Ying Khoo[1,2], Xinlin Li[1,2], Hong Zhao[2], Theodore E. Sarris[2,3], Zheng Xiang[2], Kun Zhang[1,2], Adam C. Kellerman[4], and J. Bernard Blake[5]

[1]Department of Aerospace Engineering Sciences, University of Colorado Boulder, Boulder, CO, USA, [2]Laboratory for Atmospheric and Space Physics, University of Colorado Boulder, Boulder, CO, USA, [3]Department of Electrical and Computer Engineering, Democritus University of Thrace, Xanthi, Greece, [4]Department of Earth, Planetary, and Space Sciences, University of California, Los Angeles, CA, USA, [5]The Aerospace Corporation, Los Angeles, CA, USA

Abstract Using Van Allen Probes' observations and established plasmapause location (Lpp) models, we investigate the relationship between the location of the initial enhancement (IE) of energetic electrons and the innermost (among all magnetic local time sectors) Lpp over five intense storm periods. Our study reveals that the IE events for ~30-keV to ~2-MeV electrons always occurred outside of the innermost Lpp. On average, the inner extent of the IE events (L_{IE}) for <800-keV electrons was closer to the innermost Lpp when compared to the L_{IE} for >800-keV electrons that was found consistently at ~1.5 R_E outside of the innermost Lpp. The IE of tens of kiloelectron volts electrons was observed before the IE of hundreds of kiloelectron volt electrons, and the IE of >800-keV electrons was observed on average 12.6 ± 2.3 hr after the occurrence of the earliest IE event. In addition, we report an overall electron (~30 keV to ~2 MeV) flux increase outside the plasmasphere during the selected storm periods, in contrast to the little change of energy spectrum evolution inside the plasmasphere; this demonstrates the important role of the plasmasphere in shaping energetic electron dynamics. Our investigation of the L_{IE}-Lpp relationship also provides insights into the underlying physical processes responsible for the dynamics of ~30-keV to ~2-MeV electrons.

1. Introduction

In the inner magnetosphere, energetic electrons (tens of kiloelectron volts to >1-MeV) are nominally trapped in two regions: the inner and the outer electron radiation belts. The inner electron radiation belt is centered near 1.5 Earth radii (R_E), as measured from the center of the Earth in the equatorial plane, whereas the outer electron belt is most intense around 4–5 R_E (e.g., Baker et al., 2013; X. Li et al., 2001). Between the inner and the outer electron radiation belts lies the *slot* region that has the lowest electron fluxes during geomagnetic quiet periods (e.g., Lyons & Thorne, 1973). However, in reality, the electron belts are constantly waning and waxing, merging with each other. The observed state of the radiation belts is a complex balance between acceleration, transport, and loss mechanisms (Reeves et al., 2003). In the present study, we focus on electron flux enhancement events and the underlying mechanisms of the observed electron dynamics in association with the plasmapause location.

Like radiation belt electron populations, the plasmasphere—a dense, cold (~1-eV) plasma region that corotates with the Earth—also exhibits a dynamic response to changes in the magnetospheric environment (Goldstein, 2006, and references therein). Its dynamics is largely controlled by the balance between corotation and convection electric fields. During times of strong convection, the plasmasphere is eroded and its outer boundary, plasmapause (Lpp), can occasionally move to $L \leq 2$ (e.g., Baker et al., 2004; Foster, Erickson, Baker, et al., 2016). As the enhanced convection recedes, the plasmapause can extend outward beyond $L = 6$ (e.g., Moldwin et al., 2002; O'Brien & Moldwin, 2003). The drastic density difference inside and outside of the plasmasphere affects various wave growth and their interactions with radiation belt electrons. Wave-particle interactions (Thorne, 2010, and references therein) can lead to violations of the adiabatic invariants, which may result in energy diffusion, radial diffusion, or pitch angle scattering. For instance, due to the low plasma density and thus higher phase velocity outside of the plasmasphere, chorus whistler waves, which reside mostly outside of the plasmapause, have been proven to be capable of accelerating hundreds of

kiloelectron volt electrons to >1-MeV electrons (e.g., Horne, Thorne, Glauert et al., 2005; Horne, Thorne, Shprits et al., 2005; Summers et al., 1998; Thorne et al., 2013). Meanwhile, electromagnetic ion cyclotron plasma waves, prominently existing near the plasmapause, serve as an efficient loss mechanism that precipitates relativistic electrons to the atmosphere (e.g., Miyoshi et al., 2008; Summers & Thorne, 2003; Xiang et al., 2017). Plasmaspheric hiss, which is highly associated with higher electron density regions and mainly found within the plasmasphere, is efficient in scattering electrons over a broad range of energies from tens to hundreds of kiloelectron volts that leads to the precipitation loss (Thorne, 2010, and therein; W. Li, Ma, et al., 2015). Although the generation mechanisms and the characteristics of these waves can be greatly different, they all share a close connection with the plasmapause location (e.g., Malaspina et al., 2016; Tetrick et al., 2017).

In the past decades, there have been several studies on the relationship between the electron enhancement and the plasmapause location. For instance, Baker et al. (2004) compared the electron flux measurements from the Solar, Anomalous, and Magnetospheric Particle Explorer (SAMPEX) with Lpp locations derived from Imager for Magnetopause-to-Aurora Global Exploration (IMAGE) observations and found that the Lpp locations tracked the inner edge of the outer radiation belt for relativistic electrons very well during the 2013 Halloween storm. Subsequent studies (e.g., Goldstein, Kanekal, et al., 2005; X. Li et al., 2006) examined the correlation between the electron enhancement and the plasmapause location over a prolonged period and demonstrated the same correlation. Particularly, X. Li et al. (2006), through studying 12-year >1-MeV electron flux measurements from SAMPEX and Combined Radiation and Release Experiment Satellite, determined that the initial penetration of >1-MeV electrons was found consistently outside of the innermost Lpp (innermost of the average Lpp values derived from the O'Brien & Moldwin, 2003, empirical plasmapause model). In contrast to >1-MeV electrons, the correlation between electron enhancements and the innermost plasmapause location for tens and hundreds of kiloelectron volt electrons are not as well studied. With the launch of Van Allen Probes, high energy and temporal resolution measurements of electrons from electron volts to megaelectron volts have become available; this offers an unprecedented opportunity to explore the relationship between initial electron enhancements and the innermost plasmapause location for tens and hundreds of kiloelectron volt electrons, which is the main goal of this study.

In the present study, we establish energy dependence relationships between the initial electron enhancement and the innermost Lpp for ~30-keV to ~2-MeV electrons. For the first time, we determine a remarkably consistent relationship between electron enhancements and the innermost plasmapause location over a wide range of electron energies (~30 keV to ~2 MeV): the L_{IE} of energetic electrons in the above energy range is always observed to be outside of the innermost Lpp, which are derived from the established Lpp models (Goldstein et al., 2014; X. Liu, Liu, et al., 2015). We further quantify the relationship between the initial electron enhancements and the innermost Lpp, both spatially and temporally, to shed light into the physical mechanisms behind the initial enhancements (IEs) of radiation belt electrons. A drastic difference of the energy spectrum evolution between inside and outside of the plasmasphere during storm periods is also reported in this study.

The remainder of the paper is organized as follows: Section 2 illustrates the methodology of the study, including descriptions of the plasmapause models and an overview of the observations. Section 3 discusses our findings, detailing the quantification of the correlation between the electron enhancements and the plasmapause as well as the analysis of the energy spectrum evolution inside and outside of the plasmasphere. Finally, a summary of key findings is provided in section 4.

2. Methodology

2.1. Plasmapause Models

In this study, the model-derived Lpp is preferred over the observational Lpp because the Lpp model can offer higher time resolution Lpp for all magnetic local time (MLT) sectors, unlike the observational Lpp that is constrained by the orbit/period of the active spacecraft. Often, these spacecraft only encounter the plasmapause twice in each orbit. For instance, supposed measurements from Van Allen Probes, which are in the geostationary-transfer orbit with a ~9-hr orbital period, were employed to determine the plasmapause locations, then the observational Lpp can only be identified at a specific MLT sector in each pass that is separated by an interval of ~2 to 6 hr. However, the Lpp dynamics varies within a timescale of an hour or less under

strong convection conditions. Thus, the observational Lpp is not sufficient to identify the innermost Lpp among all MLT sectors, especially during active periods. Consequently, the model-derived Lpp location is a more desirable choice in the present study.

Two Lpp models are used in this study: X. Liu, Liu, et al. (2015) model and the Plasmapause Test Particle simulation (Goldstein et al., 2014). The Liu et al. model is a multivariate plasmapause empirical model based on observations from the Time History of Events and Macroscale Interaction during Substorms (THEMIS) mission. Using 5 years of THEMIS measurements (from 2009 to 2013), Liu et al. determined 5,878 plasmapause crossings and used these crossings to establish the empirical model. In their study, a plasmapause crossing was identified by a change in plasma density by a factor of 5 within $\Delta L \leq 0.5$, which is a criterion commonly used in the related studies (e.g., Carpenter & Anderson, 1992; Moldwin et al., 2002; O'Brien & Moldwin, 2003). This empirical model uses 5-min averaged *Sym-H*, *AL*, and *AU* indices and hourly averaged *AE* and *Kp* indices as inputs and provides Lpp outputs for all MLT sectors on a timescale as short as 5 min. Overall, the Liu et al. model demonstrated a good agreement with observations, particularly before and after the storm (e.g. See Figures 7 and 9 in X. Liu, Liu, et al., 2015). During the storm period, the model-derived Lpp can reproduce the IMAGE observational Lpp locations very well on the dawnside, which is often associated with the innermost Lpp location during active periods (e.g., X. Liu, Liu, et al., 2015; O'Brien & Moldwin, 2003), with differences less than 0.5 R_E. The model performance during the refiling/recovery phase is not as good as the predicted Lpp locations that are often 1.5 to 2 R_E higher than the observations. An additional caveat in this model is that it does not reproduce the plasmaspheric plume structure and the plasmaspheric boundary layer structure. Nonetheless, this does not affect the result of our analysis since our focus is on the innermost Lpp.

Another plasmapause model used in this study is the plasmapause test particle simulation (Goldstein et al., 2014). The plasmapause in that model is represented as an ensemble of cold test particles under the influence of the E × B drift. This simulation is driven by the Volland-Stern convection electric field model (Stern, 1975; Volland, 1973) and an analytical electric field model (Goldstein, Burch, & Sandel, 2005) of the subauroral polarization stream. Inputs to the model are the solar wind electric field, the solar wind-driven magnetospheric electric field, and the *Kp* index. Despite its simple setup, the Goldstein et al. (2014) model has successfully simulated 92% of the virtual plasmapause encounters by Van Allen Probes from 15 to 20 January 2013 (See Figure 5 in Goldstein et al., 2014). Generally, the plasmapause from the Goldstein et al. model performs better during storm periods when convection is stronger than during the recovery and quiet periods. This model-observation discrepancy is taken into account when analyzing the findings in this study.

In the present study, we emphasize the need to identify the innermost Lpp in order to uncover the correlation between electron enhancements and the plasmapause. Accordingly, we first determined the innermost Lpp among all MLT sectors for each time step (15-min resolution) as the innermost Lpp. To capture the actual innermost Lpp locations that are not easily reproduced through the plasmapause models especially during the recovery phase where the strong convection recedes, we identified the innermost Lpp within 6-, 12-, and 24-hr periods (Figure 1). In general, 6- and 12-hr innermost Lpp capture the overall pattern of the innermost Lpp well, in contrast to the 24-hr innermost Lpp. At certain instances (e.g., 00:00 to 12:00 UT on 17 March 2013 in Figure 1), 6-hr innermost Lpp does a better job in tracing the innermost Lpp variations. However, unlike the 12-hr innermost Lpp, 6-hr innermost Lpp is also more likely to be subjected to the slight dynamic variation of the Lpp locations as illustrated from 12:00 to 20:00 UT on 18 March 2013 (the cyan lines) in Figure 1. To determine the optimal choice of the innermost Lpp, we have performed the analysis using 6-hr (Figures S1 and S2 in the supporting information) and 12-hr innermost Lpp and verified that they both yield very similar results. Nonetheless, since the 12-hr innermost Lpp produces a more consistent (with slightly lower uncertainties) outcome, the analysis results using 12-hr Lpp are reported in this study.

2.2. Overview of the Observation From January 2013 to July 2015

In the present study, we employ high temporal and energy resolution electron flux data from Magnetic Electron Ion Spectrometer (MagEIS) aboard the Van Allen Probes A and B (Blake et al., 2013). There are four MagEIS spectrometers on each spacecraft: one low-energy unit (20–240 keV), two medium-energy units (80–1,200 keV), and one high-energy unit (800–4,800 keV). We focused on MagEIS spin-averaged electron flux data from 30 keV to 2 MeV in this study.

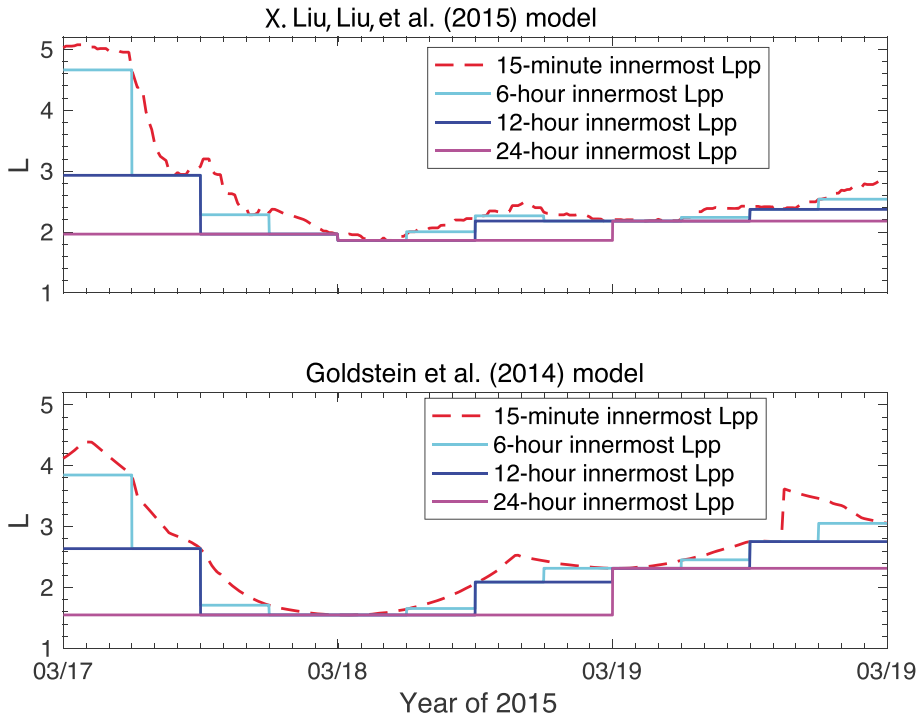

Figure 1. Comparison of 15-min, 6-hr, 12-hr, and 24-hr binned innermost Lpp derived from X. Liu, Liu, et al. (2015) model (top panel) and Goldstein et al. (2014) model (bottom panel) during the 17–20 March 2015 storm period.

MagEIS electron flux data are commonly subjected to two major sources of background contamination (Claudepierre et al., 2015): inner belt energetic protons and the bremsstrahlung X-ray radiation by multi-MeV electrons. Generally, the trapped > 10-MeV proton in the inner belt that reside at $L < 2.5$ can contaminate/affect all energetic electron measurements (e.g., X. Li, Selesnick, et al., 2015). However, lower energy electrons, particularly tens of kiloelectron volt electrons, at $L < 2.5$ are mostly unaffected by the background correction algorithms (Claudepierre et al., 2015) because their high flux level at $L < 2.5$ dominates over the contaminations caused by inner belt energetic protons. In fact, the background contamination of the energetic inner belt protons is more apparent for >500-keV electrons due to the relatively low fluxes of >500-keV electrons in the inner zone (e.g., Reeves et al., 2016). Meanwhile, the bremsstrahlung effect caused by > 1-MeV electrons is mostly responsible for the contamination of ~30- to 500-keV electron flux measurements near the heart of the outer radiation belt ($L \sim 4$). Even though the background-corrected MagEIS electron data are valuable for analysis, they are not always available. As stated in Claudepierre et al. (2015), the background correction is not possible when the low- and medium-energy units of the MagEIS instrument are in the high-rate mode or sample mode. In addition, the background correction for three out of the nine low- and medium-energy channels is not available as discussed in Claudepierre et al. (2015). Therefore, background-corrected electron flux measurements are used in this study only to validate and support the observations made using the non-background-corrected MagEIS electron flux data.

An overview of the Van Allen Probe-A MagEIS spin-averaged electron fluxes from January 2013 to July 2015 is exhibited in Figure 2. In the first three panels, the color-coded electron fluxes are plotted as a function of time and L, where L is the radial distance in Earth radii at which the dipole magnetic field line crosses the magnetic equatorial plane. By superimposing the 10-day innermost Lpp on the electron fluxes plots, we observe that electron enhancements for 1,016-keV electron energy channel (Figure 2c) occurred mostly outside of the 10-day binned innermost Lpp locations in both Lpp models at all time. This relationship is also evident in the 183-keV electron energy channel, primarily during quiet periods (Figure 2b). However, the relationship between electron enhancements and the innermost Lpp is not easy to identify during geomagnetically active periods (e.g., the time periods indicated by magenta boxes in Figure 2b).

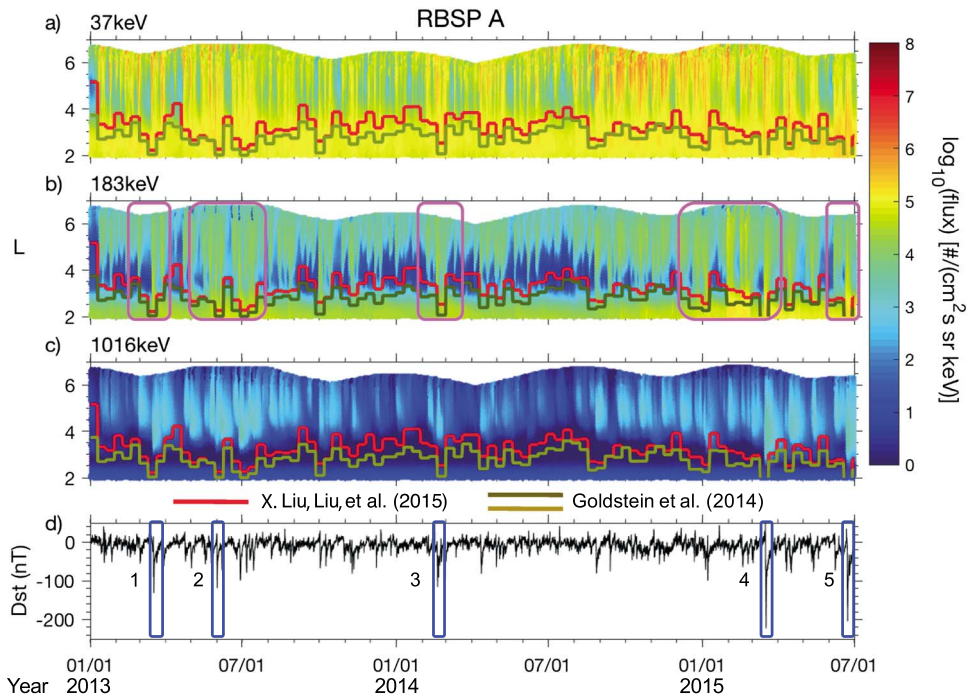

Figure 2. (a–c) Spin-averaged electron fluxes for the 37-, 183-, and 1,016-keV energy channels obtained from Magnetic Electron Ion Spectrometer aboard the Van Allen Probes-A, from January 2013 to July 2015. The gold (and dark gold) and red solid lines are the 10-day binned minimum plasmapause locations from the Goldstein et al. (2014) model and X. Liu, Liu, et al. (2015) model, respectively. The magenta boxes in the second panel show examples of periods when the spatial relationship between the plasmapause location and electron enhancements cannot be easily identified. (d) *Dst* index for the above period where blue boxes and the corresponding numbering indicate five storm time periods that are studied herein. RBSP = Radiation Belt Storm Probes.

To further investigate the correlation between the electron enhancement and the innermost Lpp during geomagnetically active periods, we draw our attention to five intense storm periods with minimum *Dst* index below −110 nT (see the highlighted blue boxes in Figure 2d and Table 1) and study the enhancement events that occurred during these periods in further detail. An overview of the statistical values of the *Dst* and *AE* indices as well as the solar wind velocity over these five periods can be found in Table 1. Common characteristics of the studied periods are that (1) they are mainly driven by coronal mass ejections (CMEs) and are associated with strong interplanetary shocks (e.g. Baker et al., 2014, 2016; Ghamry et al., 2016) and (2) they have a ≥5-day quiet period (with $Dst > -50$ nT) prior to the onset of the magnetic storms.

3. Results

3.1. IE Definition and Observations During the Five Storm Periods

In the following, we address how initial electron enhancements vary with respect to the innermost Lpp during geomagnetically storm periods. We first identify enhancement events using the following criteria: (1) an order of magnitude or more increase of electron fluxes must be observed by the same spacecraft in two consecutive passes at the same L (±0.01) and (2) these enhancements must also be seen in a larger L range ($\Delta L > 1$) with an L bin size of ±0.1, in order to avoid the discrepancies that might be introduced by the magnetic latitude variation of the satellite observations due to the tilted offset of the Earth's dipole. If two enhancement events are identified in the same pass (but at different L shells), only the enhancement event at the lower L shell is kept since our aim is to study the inner extent of the enhancement event. The first enhancement event observed by both spacecraft for the same energy channel in each storm is identified as the IE event, and the inner extent (lowest L shell) of the IE event is known as L_{IE}. In other words, there is only one IE event (and hence one L_{IE}) for a given electron energy during a storm period.

Table 1
Statistical Values of the Geomagnetic Indices (Dst, AE) and Solar Wind Velocity (V_{sw}) for the Five Storm Periods Under Investigation.

Parameters		Storm 1	Storm 2	Storm 3	Storm 4	Storm 5
		Storm periods				
		17–22 March 2013	1–4 June 2013	18–21 February 2014	17–22 March 2015	21–24 June 2015
Dst (nT)	Minimum	−132.0	−119.0	−116.0	−223.0	−204.0
	Mean	−46.9	−35.0	−43.8	−73.9	−55.0
	Median	−39.0	−26.0	−45.0	−66.0	−56.0
	Standard deviation	28.0	26.3	25.3	49.3	60.4
AE (nT)	Maximum	1822.0	1,217.0	1,236.0	1570.0	1636.0
	Mean	251.0	347.7	361.2	467.0	383.2
	Median	71.0	315.0	317.0	408.0	230.0
	Standard deviation	350.8	238.2	283.0	319.3	371.9
V_{sw} (km/s)	Maximum	725.0	774.0	691.0	683.0	742.0
	Mean	522.1	632.6	487.9	574.9	499.8
	Median	499.5	639.0	504.5	576.0	555.5
	Standard deviation	79.2	92.1	79.1	50.0	148.8

Note. The storm numbers correspond to that indicated in Figure 2d.

Figure 3 illustrates how the L_{IE} (highlighted as the yellow triangles) are identified and how they are compared with the innermost Lpp locations during the 17–20 March 2015 storm period. From Figure 3, several features are noted: (1) L_{IE} for ~30 keV to ~2-MeV electrons is often located outside of the innermost Lpp; (2) L_{IE} for tens/hundreds of kiloelectron volt electrons happens more promptly after the onset of the geomagnetic storms, as compared to >1-MeV electrons; (3) Lpp derived from the Goldstein et al. (2014) model (marked by a dashed blue line in Figure 3) are often located at lower *L* shells than the Lpp derived from X. Liu, Liu, et al. (2015) model, particularly during times of strong convection that can be inferred from the steep *Dst* gradient in Figure 3d. It is also worth noting that the definition of *L* shell during strong convection periods is less certain, particularly for tens of kiloelectron volt electrons. However, it does not qualitatively affect the general observations we made.

To further quantify the correlation between L_{IE} and Lpp, we plot the identified L_{IE} from the five studied storm periods against the innermost Lpp in Figure 4. Based on our IE definition, we identified a total of 64 IE events (and 64 corresponding L_{IE}) for ~30-keV to ~2-MeV electrons over the five periods studied herein. Overall, all L_{IE} were located outside of 12-hr binned innermost Lpp locations with only one exception for the IE of 54-keV electron during 21–24 June 2015 storm period. More specifically, the outlier is found at 0.02 and 0.09 R_E inside of the 12-hr innermost Lpp locations from the X. Liu, Liu, et al. (2015) model and the Goldstein et al. (2014) model, respectively. The strong correlation between electron enhancements and the innermost Lpp in Figure 4 is not a mere coincidence but an indication that plasmaspheric structures (and the underlying mechanisms for their formation) are important in controlling the dynamics of energetic electrons. Since different electron populations are subject to different acceleration mechanisms, it is necessary to understand the energy dependence of the relationship between the initial electron enhancement and the innermost Lpp, in order to uncover the underlying physical mechanisms.

3.2. Energy Dependence of the Spatial and Temporal Relationship Between L_{IE} and Innermost Lpp

We next investigate how the relationship between the L_{IE} and the innermost Lpp varies with electron energy, both spatially and temporally. First, we compute the spatial displacement between the L_{IE} and the model-derived 12-hr innermost Lpp as ΔL_{min}, and we average the computed ΔL_{min} for electrons with a specific energy among all five storms. The results are plotted in Figure 5a (based on X. Liu, Liu, et al., 2015, model) and Figure 5b (Goldstein et al., 2014, model), where positive ΔL_{min} refers to the distance outside of the plasmapause and negative ΔL_{min} indicates the distance inside of the plasmapause. We also investigate how the

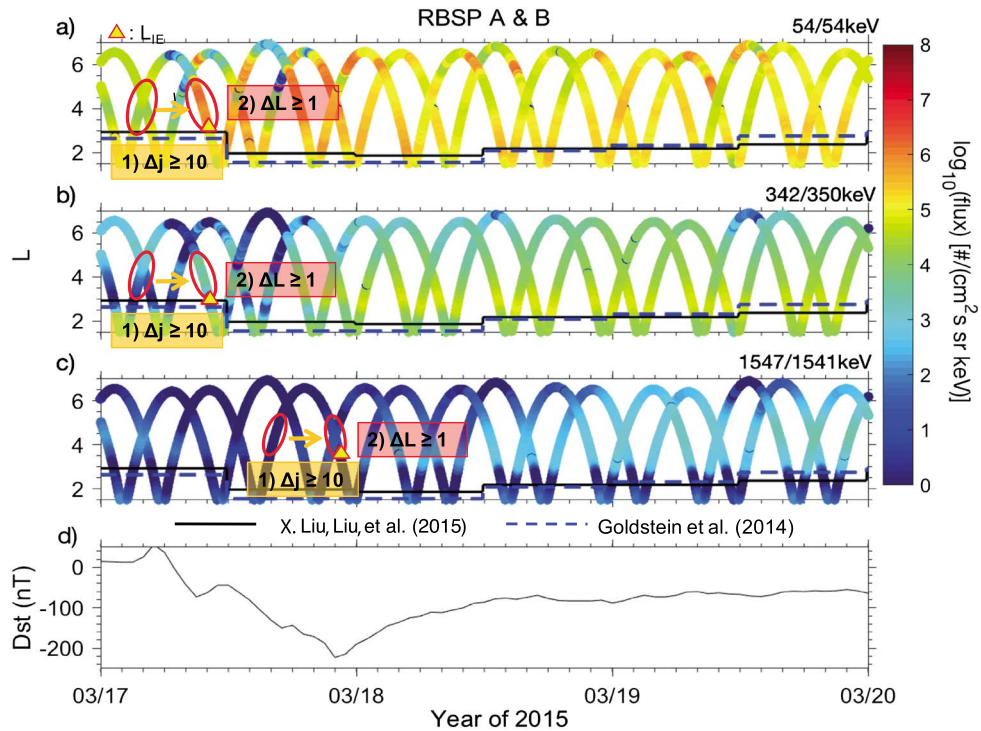

Figure 3. (a–c) Spin-averaged electron fluxes data from Magnetic Electron Ion Spectrometer onboard the Van Allen Probes-A and Van Allen Probes-B for 17–20 March 2015 with the superimposed 12-hr innermost plasmapause locations. An enhancement event is characterized by two criteria: (1) an order of more flux increase is observed between two subsequent passes of the same spacecraft ($\Delta j \geq 10$), as indicated by the orange arrows; and (2) these enhancements must be seen over a larger L range, $\Delta L \geq 1$ (highlighted by the red circled regions. The yellow triangles represent the inner edge of the initial enhancement events (L_{IE}). The solid black line refers to the 12-hr innermost Lpp from X. Liu, Liu, et al. (2015), and the dashed blue line indicates the 12-hr innermost Lpp from the plasmapause test particle simulation (Goldstein et al., 2014). (d) Corresponding *Dst* values for the 17–20 March 2015 storm period. RBSP = Radiation Belt Storm Probes.

occurrence time of the corresponding L_{IE} varies with electron energy (Figure 5c). Δt_{min} is defined as the temporal difference between the time (t_0) when the earliest L_{IE} among all energy electrons occurs and the time (t) when the L_{IE} is identified for each energy population. After obtaining the distinctive Δt_{min} ($t - t_0$) for each storm period, we determined the average Δt_{min} for each energy population over five storm periods, as shown in Figure 5c.

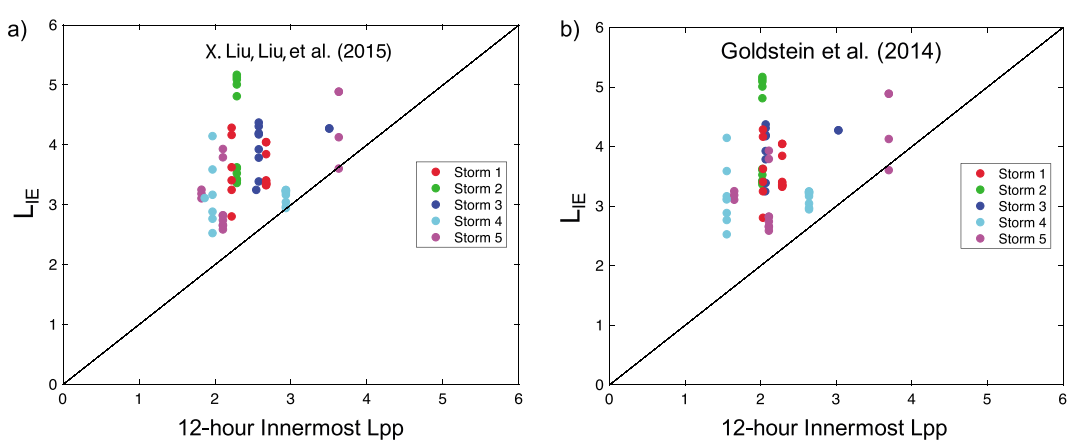

Figure 4. Comparison of the inner extent of the electron enhancement events (L_{IE}) and the 12-hr innermost Lpp using the X. Liu, Liu, et al. (2015) model (a) and the Goldstein et al. (2014) model (b). The five colors here represent the five different storm periods (also refer to Table 1).

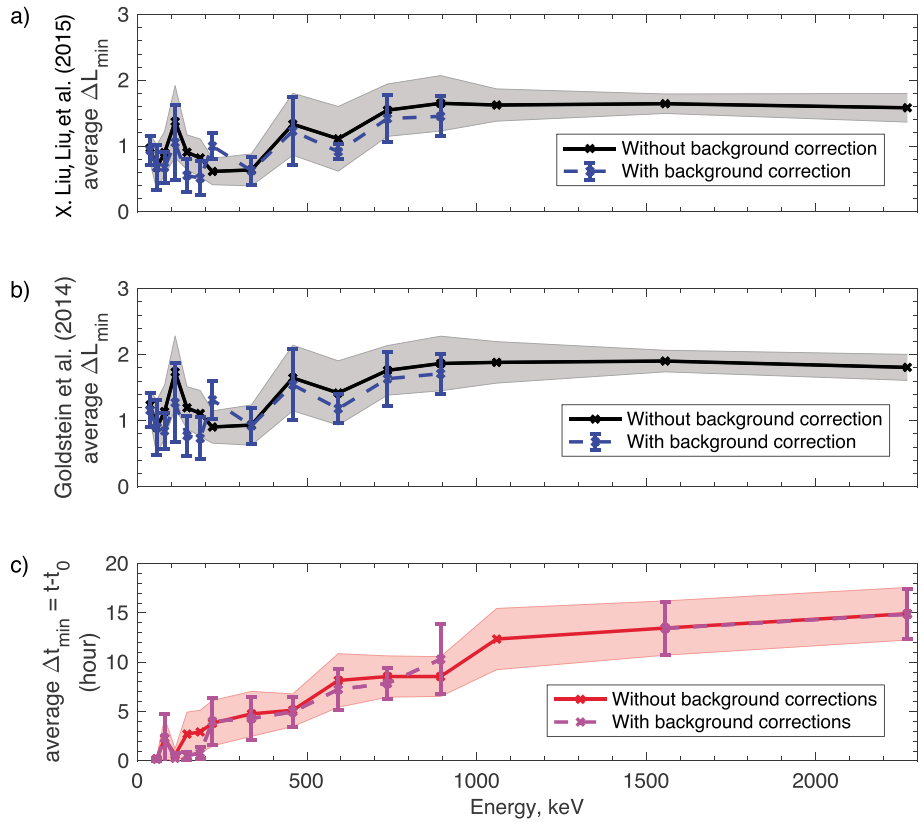

Figure 5. (a) Average $\Delta L_{\min}$ in the X. Liu, Liu, et al. (2015) model, (b) average $\Delta L_{\min}$ in the Goldstein et al. (2014) model, and (c) average $\Delta t_{\min}$ among the five storm periods against electron energies using uncorrected (solid line) and corrected (dashed line) Magnetic Electron Ion Spectrometer (MagEIS) electron fluxes data, where $\Delta t_{\min}$ represents the temporal difference between the time when the inner edge of L_{IE} is identified (t) and the time when the earliest initial enhancement (IE) event occurs among all energy electrons (t_0). The shaded areas (for uncorrected MagEIS data) and error bars (for corrected MagEIS data) in all three panels represent the 95% confidence interval of the computed average values.

The 95% confidence interval in Figure 5 is illustrated as the shaded area for the non-background-corrected MagEIS electron flux data. It is computed by multiplying the standard error (SE) of the mean with a constant, 1.96. The value of 1.96 is based on the fact that the Z-score (the number of standard deviations away from the mean) for 95% of the area of a normal distribution is 1.96. SE is calculated using the equation $\mathrm{SE} = \frac{\mathrm{SD}_i}{\sqrt{n_i}} = \frac{S_{\mathrm{pooled}}}{\sqrt{k}}$. The pooled standard deviation, $S_{\mathrm{pooled}} = \sqrt{\frac{\sum_{i=1}^{k}(n_i-1)\mathrm{SD}_i^{\,2}}{\sum_{i=1}^{k} n_i - k}}$, derived from Cohen (1988), is to determine the weighted average of the standard deviation for two or more electron energy/population, where SD_i represents the standard deviation of a certain electron population, n_i refers to the number of samples for each electron population, and k is the total number of electron populations. The superimposed dashed line and error bars in Figure 5 represent average $\Delta L_{\min}$ or $\Delta t_{\min}$ and the corresponding 95% confidence interval computed using background-corrected electron fluxes. There is a data gap in the superimposed blue dashed line (Figure 5) as the background fit for 1-MeV electron range cannot be determined due to instrument design limitations (Claudepierre et al., 2015). Regardless of some slight discrepancies, the overall trends in Figure 5 from background-corrected (blue dashed lines) and non-background-corrected (black solid lines) electron fluxes data are matching; this indicates that the correlations found in Figure 5 are not due to any background issues but some physical mechanisms.

When comparing Figures 5a and 5b, we noted that $\Delta L_{\min}$ derived from the X. Liu, Liu, et al. (2015) model (Figure 5a) is smaller (or closer to the plasmapause locations) than $\Delta L_{\min}$ obtained from the Goldstein et al. (2014) model (Figure 5b). This is consistent with our observation in Figure 3 that the Goldstein et al. (2014) model always estimates Lpp to be at lower L shells during strong convection periods when compared to

the Lpp derived from X. Liu, Liu, et al. (2015) model. Since most of the IE events occurred during the storm main phase with strong convections, the L_{IE} was often further away from the Lpp locations derived from the Goldstein et al. (2014) model than the Lpp locations derived from the X. Liu, Liu, et al. (2015) model. Nevertheless, both cases (Figures 5a and 5b) exhibit a very similar and interesting trend: the average ΔL_{min} varies drastically for lower energy electrons (<200 keV) and is then transitioned to a relatively stable average ΔL_{min} for >800-keV electrons. More specifically, the L_{IE} for <800-keV electrons often lies closer to the 12-hr innermost Lpp than that for >800-keV electrons. Among all electron populations, ~200- to 300-keV electron have the lowest average ΔL_{min}, which is at 0.70 ± 0.18 and 0.99 ± 0.22 R_E away from 12-hr innermost Lpp from the X. Liu, Liu, et al. (2015) and the Goldstein et al. (2014) models, respectively, as derived from corrected and uncorrected electron fluxes. We also observe that the average ΔL_{min} for <800 keV is associated with a more drastic variation and with a wider 95% confidence interval, or in other words, with a higher uncertainty of the computed average ΔL_{min}. This is partly due to the small sample size (the maximum sample size for each energy channel in this study is five, which corresponds to the five storm periods). Besides, various mechanisms like convective transport, substorm injections, and chorus wave activities might act on <800-keV electrons, and the complicated, combined effect of these mechanisms could contribute to the higher variations of ΔL_{min} for <800 keV.

Since the plasmapause location is a result of the balance between the corotational E × B drift and the sunward E × B drift that is closely associated with enhanced convection (Goldstein, 2006, and references therein), our observations suggest that the same enhanced convection responsible for plasmasphere erosion could account for the flux enhancements of lower energy electrons. Simulations from previous studies (Korth et al., 1999; S. Liu et al., 2003; Thorne et al., 2007; Zhao et al., 2017) have suggested that <200-keV electrons are more likely to be radially transported inward by enhanced convective electric fields in the slot region, around $3 < L < 5$. Using test particle simulations, Califf et al. (2016) showed that convective transport by the large scale of electric fields in the order of 1 to 2 mV/m can explain the flux enhancement of hundreds of kiloelectron volt electrons at $L \sim 3$ during the February 2014 storm that is also examined herein. During the 1 June 2013 storm event, which is another event that is studied in this paper, Thaller et al. (2015) reported the appearance of a large duskward electric field in the order of 1 to 2 mV/m. They determined that this enhanced convection electric field can contribute to the ring current formation, by radially transporting few kiloelectron volt ions inward from the plasma sheet to lower L shells and that it can also contribute to the erosion of the plasmasphere. Although Thaller et al. (2015) did not provide direct evidence that relates enhanced convection electric fields to electron flux enhancements in the slot region, we can infer from the simulation conducted by Califf et al. (2016) that the observed 1- to 2-mV/m electric field enhancement is also capable of transporting <200-keV electrons inward. Combined with the results from previous studies, the observations presented herein indicate that the same convective electric field responsible for the erosion of the plasmasphere also plays an important role in the dynamics of <200-keV electrons, potentially transporting the critical electron seed population radially inward during strong convection periods.

Another interesting feature is the relatively stable average ΔL_{min} that is observed for relativistic (>800-keV) electrons (Figures 5a and 5b). On average, L_{IE} for >800-keV electrons, as derived from both corrected and uncorrected flux data, are constantly found 1.56 ± 0.22 and 1.81 ± 0.22 R_E from the innermost Lpp locations derived using the X. Liu, Liu, et al. (2015) model and the Goldstein et al. (2014) model. Besides, the L_{IE} for >800-keV electrons were identified on average 12.6 ± 2.3 hr after the earliest L_{IE} identified in the lower energy electron channel. The late occurrence of relativistic electron flux enhancements and the constant spatial difference between L_{IE}-Lpp for relativistic electrons are coherent with the proposed mechanism of local acceleration of the seed population (tens to a few hundred kiloelectron volt electrons) by chorus waves, as discussed by previous studies such as Horne, Thorne, Glauert, et al. (2005), Reeves et al. (2013), and Jaynes et al. (2015).

According to studies like Horne, Thorne, Glauert, et al. (2005), Summers et al. (2007), and Thorne et al. (2013), chorus waves that reside outside the plasmapause are most efficient in locally accelerating hundreds of kiloelectron volt electrons to relativistic (>1-MeV) energies with acceleration timescales ≤1 day. Several past studies (e.g., Foster et al., 2014; Foster, Erickson, Omura, et al., 2016; W. Li et al., 2014; S. Liu, Xiao et al., 2015; Xiao et al., 2014) analyzed the relativistic electron dynamics over the five intense storm periods that we examined in this paper using observations/simulations; they concurrently attributed chorus wave as an important

contributor to the relativistic electron enhancements. For instance, W. Li et al. (2014) and Xiao et al. (2014) conducted two independent studies on the March 2013 storm period, the same storm period studied in this paper, using simulation driven by chorus waves only and chorus wave/radial diffusion, respectively. Both papers highlighted the importance of chorus-driven acceleration in reproducing $>$1-MeV electron flux enhancements at $L \sim 4$ that occurred ~12–15 hr later after the onset of the storm. Likewise, Boyd et al. (2018) examined 80 outer belt enhancement events from October 2012 to April 2017 using Van Allen Probes and THEMIS data. Not only did they find that local acceleration is the dominant acceleration mechanism for equatorially mirroring electrons with μ = 700 MeV/G, which translates to ~1-MeV electrons at $L = 5$, but they also determined that the locations of the growing phase space density peak, which is a signature of local acceleration, are all found outside of the plasmapause locations. Those results are supportive of our observations for $>$800-keV electron enhancements as described in Figure 5. Since the local acceleration is most effective outside of the plasmapause locations (e.g., Horne, Thorne, Shprits, et al., 2005), our observations, along with the previous literature, clearly demonstrate and are in agreement with that the local acceleration is the dominant acceleration mechanism that contributes to the IEs of $>$800-keV electrons.

When studying the enhancement in the fluxes of energetic ($>$30-keV) electrons, it is also necessary to consider the effect of ultralow-frequency (ULF) waves on these electrons. Various previous studies showed that the increase in energetic electron flux is often observed in association with enhanced ULF wave activities (Elkington, 2006, and references therein). It is noteworthy that the five storm periods studied in this paper are all CME-driven storms and are associated with strong interplanetary shocks. Since the strong interplanetary shock is an important driver for the generation of ULF waves, the latter is expected to play a role in the observed electron dynamics in this study. Previous studies have discussed how ULF wave-driven radial diffusion can transport hundreds of kiloelectron volt electrons into lower L shells (e.g., Pokhotelov et al., 2016; Shprits et al., 2008). It is conceivable that the enhancements of the energetic (hundreds of kiloelectron volts to $>$1-MeV) electrons are due to inward radial transport associated with ULF waves.

3.3. Energy Spectrum Inside and Outside of the Plasmasphere

A statistical analysis was conducted to understand the overall energy spectrum evolution inside and outside of the plasmasphere during the five storm periods. In Figure 6a, we plot the electron energy spectra at $L = 1.5 \pm 0.01$ at times $t_{\mathrm{min(Dst)}}$ and t_{bef}, where $t_{\mathrm{min(Dst)}}$ represents the time when the *Dst* value reaches its minimum during the storm period and t_{bef} refers to 24 hr before $t_{\mathrm{min(Dst)}}$. At both time instances, these spectra (at $L = 1.5$) are located inside of Lpp. We observe little variations of ~30-keV to ~2-MeV electron fluxes before and during the storm. In Figure 6b, the measured spectra at $L = 3 \pm 0.01$ are located within the plasmasphere at t_{bef}, but outside of the plasmasphere at $t_{\mathrm{min(Dst)}}$ (this is true for all five storms that are studied in this study. See Figures S1 to S5 in the supporting information for more information). An increase in the electron flux is observed for all electron energies up to ~2 MeV, with larger flux enhancements occurring in the electron range from ~300 to ~500 keV. However, it is still unclear, based on our observation alone, whether the observed vast difference in the energy spectrum between inside (before the storm) and outside (during the storm) of the plasmasphere in Figure 6b is a result of the strong flux enhancements during storms and/or is an implication of how the plasmasphere can shape dramatically different energy spectra inside/outside the plasmasphere.

A similar analysis using background-corrected data (not shown here) was also conducted. Even though the observed energy spectrum using background-corrected measurements are relatively sparse (due to data gap), we still observe a similar drastic flux increase when the energy spectrum fell outside of the plasmasphere during storm time, in contrast to the little change of the energy spectrum at the L shell inside of the Lpp; this further validates our observations in Figure 6. Besides the statistical analysis, we also analyze how the energy spectrum varies from $L = 1.5$ to $L = 3.5$ for the five storm periods and observe the same pattern as noted in the statistical analysis (Figure 6). The details of the energy spectra evolution from $L = 1.5$ to $L = 3.5$ for each storm period can be found in the supporting information (Figures S3 to S7). In short, the striking difference of the energy spectrum evolution between inside and outside of the plasmasphere during storm periods serves as another piece of supporting evidence to illustrate the important role of the plasmasphere in shaping the dynamics of energetic electrons from ~30 keV to ~2 MeV.

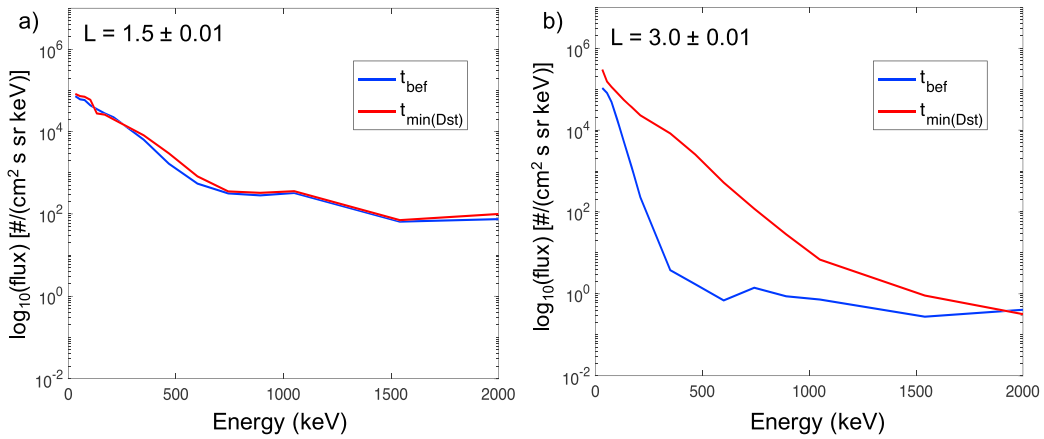

Figure 6. Statistical analysis of the energy spectrum before and during the five intense storm periods at $L = 1.5$ (a) and 3 (b). The blue solid line represents the energy spectrum before the storm periods (t_{bef}), and the red line depicts the energy spectrum during the storm periods ($t_{min(Dst)}$).

4. Conclusion

In the present study, we investigated the relationship between the IE of ~30-keV to ~2-MeV electrons and the innermost plasmapause locations. Over the five CME-driven geomagnetic storm periods, we presented the first comprehensive evidence that the IE of ~30-keV to ~2-MeV electrons is persistently outside the innermost plasmapause locations. These findings are suggesting that enhanced convection is the dominant mechanism in transporting <200-keV electrons into lower L shells, while local acceleration due to chorus waves predominantly controls the relativistic (>800-keV) electron enhancements, which always occur ~12.6 hr later (than the earliest IE events) at ~1.56 and ~1.81 R_E away from the innermost Lpp locations derived from the X. Liu, Liu, et al. (2015) model and the Goldstein et al. (2014) model, respectively. A drastic difference of the energy spectrum evolution between inside and outside of the plasmasphere further attests the significant role of the plasmasphere in affecting the dynamics of energetic electrons in a wide energy range, ~30 keV to ~2 MeV, during intense storm periods. Lastly, it is also important to note that this study focuses only on active periods with strong convections that are driven by CME events. Therefore, it would be interesting to investigate corotating interaction region or high-speed stream-driven storm periods in the future study; this will provide a more comprehensive understanding of the relationship between electron enhancements and the plasmapause location under various solar wind conditions.

Acknowledgments
This work was supported in part by NASA grants NNX15AF56G and 80NSSC18K1119 and by NASA/RBSP-ECT funding through JHU/APL contract 967399 under prime NASA contract NAS5-01072. We thank Alison Jaynes, Trevor Leonard, Wenlong Liu, and Binbin Ni for the helpful discussion. All Van Allen Probes Level-2 data and the Goldstein et al. (2014) plasmapause simulation outputs are publicly available at www.rbsp-ect.lanl.gov. The MATLAB code for the X. Liu, Liu, et al. (2015) plasmapause model is provided as the supporting information Software 1 at https://agupubs.onlinelibrary.wiley.com/doi/abs/10.1002/2015JA021801. The solar parameters and geomagnetic indices used in this study are obtained from the OMNI database (http://omniweb.gsfc.nasa.gov).

References

Baker, D. N., Jaynes, A. N., Kanekal, S. G., Foster, J. C., Erickson, P. J., Fennel, J. F., et al. (2016). Highly relativistic radiation belt electron acceleration, transport, and loss: Large solar storm events of March and June 2015. *Journal of Geophysical Research: Space Physics*, *121*, 6647–6660. https://doi.org/10.1002/2016JA022502

Baker, D. N., Jaynes, A. N., Li, X., Henderson, M. G., Kanekal, S. G., Reeves, G. D., et al. (2014). Gradual diffusion and punctuated phase space density enhancements of highly relativistic electrons: Van Allen Probes observations. *Geophysical Research Letters*, *41*, 1351–1358. https://doi.org/10.1002/2013GL058942

Baker, D. N., Kanekal, S. G., Hoxie, V. C., Henderson, M. G., Li, X., Spence, H. E., et al. (2013). A long-lived relativistic electron storage ring embedded in Earth's outer Van Allen belt. *Science*, *340*(6129), 186–190. https://doi.org/10.1126/science.1233518

Baker, D. N., Kanekal, S. G., Li, X., Monk, S. P., Goldstein, J., & Burch, J. L. (2004). An extreme distortion of the Van Allen belt arising from the "Halloween" solar storm in 2003. *Nature*, *432*(7019), 878–881. https://doi.org/10.1038/nature03116

Blake, J. B., Carranza, P. A., Claudepierre, S. G., Clemmons, J. H., Crain, W. R. Jr., Dotan, Y., et al. (2013). The Magnetic Electron Ion Spectrometer (MagEIS) instruments aboard the Radiation Belt Storm Probes (RBSP) spacecraft. *Space Science Reviews*, *179*(1-4), 383–421. https://doi.org/10.1007/s11214-013-9991-8

Boyd, A. J., Turner, D. L., Reeves, G. D., Spence, H. E., Baker, D. N., & Blake, J. B. (2018). What causes radiation belt enhancements: A survey of the Van Allen Probes Era. *Geophysical Research Letters*, *45*, 5253–5259. https://doi.org/10.1029/2018GL077699

Califf, S., Li, X., Zhao, H., Kellerman, A., Sarris, T. E., Jaynes, A. N., & Malaspina, D. M. (2016). The role of the convection electric field in filling the slot region between the inner and outer radiation belt. *Journal of Geophysical Research: Space Physics*, *122*, 2051–2068. https://doi.org/10.1002/2016JA023657

Carpenter, D. L., & Anderson, R. R. (1992). An ISEE/whistler model of equatorial electron density in the magnetosphere. *Journal of Geophysical Research*, *97*(A2), 1097–1108. https://doi.org/10.1029/91JA01548

Claudepierre, S. G., O'Brien, T. P., Blake, J. B., Fennel, J. F., Roeder, J. L., Clemmons, J. H., et al. (2015). A background correction algorithm for Van Allen Probes MagEIS electron flux measurements. *Journal of Geophysical Research: Space Physics*, *120*, 5703–5727. https://doi.org/10.1002/2015JA021171

Cohen, J. (1988). *Statistical power analysis for the behavioral sciences*. New Jersey: Lawrence Erlbaum Associates.

Elkington, S. R. (2006). A review of ULF interactions with radiation belt electrons. In K. Takahashi, P. J. Chi, R. E. Denton, & R. L. Lysak (Eds.), *Magnetospheric ULF waves: Synthesis and new directions, Geophysical Monograph Series* (Vol. 169, pp. 177). Washington, DC: American Geophysical Union. https://doi.org/10.1029/169GM12

Foster, J. C., Erickson, P. J., Baker, D. N., Claudepierre, S. G., Kletzing, C. A., Kurth, W., et al. (2014). Prompt energization of relativistic and highly relativistic electrons during a substorm interval: Van Allen Probes observations. *Geophysical Research Letters*, *41*, 20–25. https://doi.org/10.1002/2013GL058438

Foster, J. C., Erickson, P. J., Baker, D. N., Jaynes, A. N., Mishin, E. V., Fennel, J. F., et al. (2016). Observations of the impenetrable barrier, the plasmaspause, and the VLF bubble during the 17 March 2015 storm. *Journal of Geophysical Research: Space Physics*, *121*, 5537–5548. https://doi.org/10.1002/2016JA022509

Foster, J. C., Erickson, P. J., Omura, Y., Baker, D. N., Kletzing, C. A., & Claudepierre, S. G. (2016). Van Allen Probes observations of prompt MeV radiation belt electron acceleration in nonlinear interactions with VLF chorus. *Journal of Geophysical Research: Space Physics*, *122*, 324–339. https://doi.org/10.1002/2016JA023429

Ghamry, E., Lethy, A., Arafa-Hamed, T., & Elaal, E. A. (2016). A comprehensive analysis of the geomagnetic storms occurred during 18 February and 2 March 2014. *NRIAG Journal of Astronomy and Geophysics*, *5*(1), 263–268. https://doi.org/10.1016/j.nrjag.2016.03.001

Goldstein, J. (2006). Plasmasphere response: Tutorial and review of recent imaging results. *Space Science Reviews*, *124*(1-4), 203–216. https://doi.org/10.1007/s11214-006-9105-y.

Goldstein, J., Burch, J. L., & Sandel, B. R. (2005). Magnetospheric model of subauroral polarization stream. *Journal of Geophysical Research*, *110*, A09222. https://doi.org/10.1029/2005JA011135

Goldstein, J., De Pascuale, S., Kletzing, C., Kurth, W., Genestreti, K. J., Skoug, R. M., et al. (2014). Simulation of Van Allen Probes plasmapause encounters. *Journal of Geophysical Research: Space Physics*, *119*, 7464–7484. https://doi.org/10.1002/2014JA020252

Goldstein, J., Kanekal, S. G., Baker, D. N., & Sandel, B. R. (2005). Dynamic relationship between the outer radiation belt and the plasma- pause during March–May 2001. *Geophysical Research Letters*, *32*, L15104. https://doi.org/10.1029/2005GL023431

Horne, R. B., Thorne, R. M., Glauert, S. A., Albert, J. M., Meredith, N. P., & Anderson, R. R. (2005). Timescale for radiation belt electron acceleration by whistler mode chorus waves. *Journal of Geophysical Research*, *110*, A03225. https://doi.org/10.1029/2004JA010811

Horne, R. B., Thorne, R. M., Shprits, Y. Y., Meredith, N. P., Glauert, S. A., Smith, A. J., et al. (2005). Wave acceleration of electrons in the Van Allen radiation belts. *Nature*, *437*(7056), 227–230. https://doi.org/10.1038/nature03939

Jaynes, A. N., Baker, D. N., Singer, H. J., Rodriguez, J. V., Loto'aniu, T. M., Ali, A. F., et al. (2015). Source and seed populations for relativistic electrons: Their roles in radiation belt changes. *Journal of Geophysical Research: Space Physics*, *120*, 7240–7254. https://doi.org/10.1002/2015JA021234

Korth, H., Thomsen, M. F., Borovsky, J. E., & McComas, D. J. (1999). Plasma sheet access to geosynchronous orbit. *Journal of Geophysical Research*, *104*(A11), 25,047–25,061. https://doi.org/10.1029/1999JA900292

Li, W., Ma, Q., Thorne, R. M., Bortnik, J., Kletzing, C. A., Kurth, W. S., et al. (2015). Statistical properties of plasmaspheric hiss derived from Van Allen Probes data and their effects on radiation belt electron dynamics. *Journal of Geophysical Research: Space Physics*, *120*, 3393–3405. https://doi.org/10.1002/2015JA021048

Li, W., Thorne, R. M., Ma, Q., Ni, B., Bortnik, J., Baker, D. N., et al. (2014). Radiation belt electron acceleration by chorus waves during the 17 March 2013 storm. *Journal of Geophysical Research: Space Physics*, *119*, 4681–4693. https://doi.org/10.1002/2014JA019945

Li, X., Baker, D. N., Kanekal, S. G., Looper, M., & Temerin, M. (2001). Long term measurements of radiation belts by SAMPEX and their variations. *Geophysical Research Letters*, *28*(20), 3827–3830. https://doi.org/10.1029/2001GL013586.

Li, X., Baker, D. N., O'Brien, T. P., Xie, L., & Zong, Q. G. (2006). Correlation between the inner edge of outer radiation belt electrons and the innermost plasmapause location. *Geophysical Research Letters*, *33*, L14107. https://doi.org/10.1029/2006GL026294

Li, X., Selesnick, R. S., Baker, D. N., Jaynes, A. N., Kanekal, S. G., Schiller, Q., et al. (2015). Upper limit on the inner radiation belt MeV electron intensity. *Journal of Geophysical Research: Space Physics*, *120*, 1215–1228. https://doi.org/10.1002/2014JA020777

Liu, S., Chen, M. W., Lyons, L. R., Korth, H., Albert, J. M., Roeder, J. L., et al. (2003). Contribution of convective transport to stormtime ring current electron injection. *Journal of Geophysical Research*, *108*(A10), 1372. https://doi.org/10.1029/2003JA010004

Liu, S., Xiao, F., Yang, C., He, Y., Zhou, Q., Kletzing, C. A., et al. (2015). Van Allen Probes observations linking radiation belt electrons to chorus waves during 2014 multiple storms. *Journal of Geophysical Research: Space Physics*, *120*, 938–948. https://doi.org/10.1002/2014JA020781

Liu, X., Liu, W., Cao, J. B., Fu, H. S., Yu, J., & Li, X. (2015). Dynamic plasmapause model based on THEMIS measurements. *Journal of Geophysical Research: Space Physics*, *120*, 10,543–10,556. https://doi.org/10.1002/2015JA021801

Lyons, L. R., & Thorne, R. M. (1973). Equilibrium structure of radiation belt electrons. *Journal of Geophysical Research*, *78*(13), 2142–2149. https://doi.org/10.1029/JA078i013p02142

Malaspina, D. M., Jaynes, A. N., Boulé, C., Bortnik, J., Thaller, S. A., Ergun, R. E., et al. (2016). The distribution of plasmaspheric hiss wave power with respect to plasmapause location. *Geophysical Research Letters*, *43*, 7878–7886. https://doi.org/10.1002/2016GL069982

Miyoshi, Y., Sakaguchi, K., Shiokawa, K., Evans, D., Albert, J., Connors, M., & Jordanova, V. (2008). Precipitation of radiation belt electrons by EMIC waves, observed from ground and space. *Geophysical Research Letters*, *35*, L23101. https://doi.org/10.1029/2008GL035727

Moldwin, M. B., Downward, L., Rassoul, H. K., Amin, R., & Anderson, R. R. (2002). A new model of the location of the plasmapause: CRRES results. *Journal of Geophysical Research*, *107*(A11), 1339. https://doi.org/10.1029/2001JA009211

O'Brien, T. P., & Moldwin, M. B. (2003). Empirical plasmapause models from magnetic indices. *Geophysical Research Letters*, *30*(4), 1152. https://doi.org/10.1029/2002GL016007

Pokhotelov, D., Rae, I. J., Murphy, K. R., Mann, I. R., & Ozeke, L. (2016). Effects of ULF wave power on relativistic radiation belt electrons: 8–9 October 2012 geomagnetic storm. *Journal of Geophysical Research: Space Physics*, *121*, 11,766–11,779. https://doi.org/10.1002/2016JA023130

Reeves, G., Spence, H. E., Henderson, M. G., Morley, S. K., Friedel, R. H. W., et al. (2013). Electron acceleration in the heart of the Van Allen radiation belts. *Science*, *341*(6149), 991–994. https://doi.org/10.1126/science.1237743

Reeves, G. D., Friedel, R. H. W., Larsen, B. A., Skoug, R. M., Funsten, H. O., Claudepierre, S. G., et al. (2016). Energy-dependent dynamics of keV to MeV electrons in the inner zone, outer zone, and slot regions. *Journal of Geophysical Research: Space Physics*, *121*, 397–412. https://doi.org/10.1002/2015JA021569

Reeves, G. D., McAdams, K. L., Friedel, R. H. W., & O'Brien, T. P. (2003). Acceleration and loss of relativistic electrons during geomagnetic storms. *Geophysical Research Letters*, *30*(10), 1529. https://doi.org/10.1029/2002GL016513

Shprits, Y. Y., Subbotin, D. A., Meredith, N. P., & Elkington, S. R. (2008). Review of modeling of losses and sources of relativistic electrons in the outer radiation belt II: Local acceleration and loss. *Journal of Atmospheric and Solar-Terrestrial Physics*, *70*(14), 1694–1713. https://doi.org/10.1016/j.jastp.2008.06.014.

Stern, D. P. (1975). The motion of a proton in the equatorial magnetosphere. *Journal of Geophysical Research*, *80*(4), 595–599. https://doi.org/10.1029/JA080i004p00595

Summers, D., Ni, B., & Meredith, N. P. (2007). Timescales for radiation belt electron acceleration and loss due to resonant wave-particle interactions: 2. Evaluation for VLF chorus, ELF hiss, and electromagnetic ion cyclotron waves. *Journal of Geophysical Research*, *112*, A04207. https://doi.org/10.1029/2006JA011993

Summers, D., & Thorne, R. M. (2003). Relativistic electron pitch angle scattering by electromagnetic ion cyclotron waves during geomagnetic storms. *Journal of Geophysical Research*, *108*(A4), 1143. https://doi.org/10.1029/2002JA009489

Summers, D., Thorne, R. M., & Xiao, F. (1998). Relativistic theory of wave-particle resonant diffusion with application to electron acceleration in the magnetosphere. *Journal of Geophysical Research*, *103*(A9), 20,487–20,500. https://doi.org/10.1029/98JA01740

Tetrick, S. S., Engebretson, M. J., Posch, J. L., Olson, C. N., Smith, C. W., Denton, R. E., et al. (2017). Location of intense electromagnetic ion cyclotron (EMIC) wave events relative to the plasmapause: Van Allen Probes observations. *Journal of Geophysical Research: Space Physics*, *122*, 4064–4088. https://doi.org/10.1002/2016JA023392

Thaller, S. A., Wygant, J. R., Dai, L., Breneman, A. W., Kersten, K., Cattell, C. A., et al. (2015). Van Allen Probes investigation of the large-scale duskward electric field and its role in ring current formation and plasmasphere erosion in the 1 June 2013 storm. *Journal of Geophysical Research: Space Physics*, *120*, 4531–4543. https://doi.org/10.1002/2014JA020875

Thorne, R. M. (2010). Radiation belt dynamics: The importance of wave-particle interactions. *Geophysical Research Letters*, *37*, L22107. https://doi.org/10.1029/2010GL044990

Thorne, R. M., Li, W., Ni, B., Ma, Q., Bortnik, J., Chen, L., et al. (2013). Rapid local acceleration of relativistic radiation belt electrons by magnetospheric chorus. *Nature*, *504*(7480), 411–414. https://doi.org/10.1038/nature12889

Thorne, R. M., Shprits, Y. Y., Meredith, N. P., Horne, R. B., Li, W., & Lyons, L. R. (2007). Refilling of the slot region between the inner and outer electron radiation belts during geomagnetic storms. *Journal of Geophysical Research*, *112*, A06203. https://doi.org/10.1029/2006JA012176

Volland, H. (1973). A semiempirical model of large-scale magnetospheric electric fields. *Journal of Geophysical Research*, *78*(1), 171–180. https://doi.org/10.1029/JA078i001p00171

Xiang, Z., Tu, W., Li, X., Ni, B., Morley, S. K., & Baker, D. N. (2017). Understanding the mechanisms of radiation belt dropouts observed by Van Allen Probes. *Journal of Geophysical Research: Space Physics*, *122*, 9858–9879. https://doi.org/10.1002/2017JA024487

Xiao, F., Yang, C., He, Z., Su, Z., Zhou, Q., He, Y., et al. (2014). Chorus acceleration of radiation belt relativistic electrons during March 2013 geomagnetic storm. *Journal of Geophysical Research: Space Physics*, *119*, 3325–3332. https://doi.org/10.1002/2014JA019822

Zhao, H., Baker, D. N., Califf, S., Li, X., Jaynes, A. N., Leonard, T., et al. (2017). Van Allen probes measurements of energetic particle deep penetration into the low L region ($L < 4$) during the storm on 8 April 2016. *Journal of Geophysical Research: Space Physics*, *122*, 12,140–12,152. https://doi.org/10.1002/2017JA024558